SUPPORTING INFORMATION

Preparation of labeled mAb stock solution

Stock solutions of fluorescently labeled mAb2 were prepared by conjugation of Atto-488 NHS ester to primary amines on the mAb surface. Briefly, a 5 mg/mL stock solution of mAb2 was buffer-exchanged into 150:150 mM $NaHCO_3$:NaCl (pH 8.3) solution using Centri-Spin 20 SEC columns (Princeton Separations, Adelphia, NJ) that had been hydrated in advance in the pH 8.3 $NaHCO_3$:NaCl buffer for 30 minutes. The mAb concentration was measured after buffer exchange using a NanoDrop 2000 UV-Vis spectrophotometer (Thermo Fisher Scientific, Waltham, MA). Atto-488 was dissolved in DMSO at 10 mM and stored at -80°C prior to use. The thawed dye was added to the pH 8.3 buffer-exchanged mAb solution at a 1:1 dye:mAb molar ratio for the labeling reaction. The amount of DMSO in the labeling reaction mixture (from the dye stock) did not exceed 1% v/v. The dye-mAb mix was kept in a dark environment (to avoid photobleaching) and allowed to react for 30 minutes at room temperature. Unreacted dye was then removed by buffer exchanging the labeled mAb solution (containing the unbound dye) back into the 21:30 mM Na:OAc (pH 5.5) solution with Centri-Spin 20 SEC columns.

The dye and mAb concentrations after buffer exchange were checked with the NanoDrop spectrophotometer. The dye absorbance was measured at 501 nm with an extinction coefficient of 90000 $M^{-1}cm^{-1}$, and the mAb absorbance was measured at 280 nm with an extinction coefficient of 213,000 $M^{-1}cm^{-1}$ (1.42 $mL*mg^{-1}cm^{-1}$ converted to molar concentration units). The absorbance at 280 nm was also corrected for contributions from the dye fluorescence ($A_{280,mAb} = A_{280,total} - 0.1*A_{501}$) prior to calculating the mAb concentration. The typical labeled mAb concentration after buffer exchange was ~25 μM, and the typical dye to mAb molar ratio was 0.7:1.

The labeled mAb solution was split into 20 μL aliquots in PCR tubes, frozen in liquid nitrogen, and kept frozen at -20°C prior to use. Aliquots were individually thawed up to 3 – 4 hours prior to their addition to unlabeled, concentrated mAb samples for fluorescence correlation spectroscopy (FCS) measurements.

Slide cleaning and passivation – wet passivation technique

Due to the high sensitivity of FCS measurements to optical artifacts introduced by dust and protein adsorption to the imaging surface, the glass cover slips used to hold the mAb samples were cleaned and passivated to resist protein adsorption. In the wet passivation technique[1, 2] (used only for the initial method development experiments), a thin liquid film of adsorbed DOPC (1,2-dioleoyl-sn-glycero-3-phosphocholine) vesicles was used to prevent protein adsorption on the glass surface. A stock solution of DOPC vesicles was prepared by first drying the DOPC solution as received from the vendor (dissolved in chloroform at 0.0127 M) under a N_2 stream and subsequently under vacuum for two hours. The dried DOPC was then reconstituted at 500 μM in the same buffer as the mAb samples (21:30 mM Na:OAc, pH 5) and probe sonicated in an ice bath to form small unilamellar vesicles. The DOPC solution was then centrifuged at 17,000g for 6 minutes to sediment metal particulates shed by the sonicator probe, and the supernatant was filtered using 0.22 μm filters into low-adhesion microcentrifuge tubes. The DOPC stock solution was stored at 4°C for up to 1 week prior to use.

The glass cover slips were cleaned by soaking in a hot (lightly steaming) solution of 2% v/v Hellmanex III cleaning detergent for 30 minutes in glass carafes. The cover slips were then flushed with an excess of ultrapure water (drain/refill the carafe 10 times with water) to remove the detergent. The cover slips were then individually washed under running ultrapure water and dried under a N_2 stream. The cleaned silicone gaskets (as described in the Methods section) were gently pressed onto the top of the cleaned cover slips to create a temporary water-tight seal to form the imaging well. 20 μL of the 500 μM DOPC stock solution was added to the well and allowed to sit for 5 minutes to generate a thin layer of adsorbed DOPC vesicles. Excess DOPC vesicles were removed by by serially rinsing the liquid in the imaging well with excess mAb buffer (21:30 mM Na:OAc), resulting in a dilution of ~16,000-fold.

Slide cleaning and passivation – dry passivation technique

An alternative dry passivation technique was used in most of the experiments in this study due to its superior performance for high concentration measurements relative to the wet passivation used in

earlier method development experiments. In the dry passivation technique, the glass cover slips were cleaned using a modified RCA protocol[3, 4] and passivated with a coupled silane-PEG layer to prevent protein adsorption.[3, 5] Briefly, the cover slips were first soaked in ethanol for 10 minutes and simultaneously sonicated to dislodge organic contaminants. The cover slips were then flushed with an excess of ultrapure water to remove all organic solvents. The cover slips were then soaked in a hot (70 - 80°C) solution of 30% hydrogen peroxide in 1.5 M KOH for 10 minutes in glass carafes to etch the glass surface. IT IS CRITICAL that all trace organic solvent (ethanol) be removed prior to addition of the peroxide/KOH mixture, as peroxide will react with the ethanol and cause explosive boiling. Similarly, the KOH/peroxide mixture should be prepared by slowly adding the peroxide to the KOH solution in order to prevent rapid, uncontrolled boiling of the mixture. The KOH/peroxide solution was then drained, and the cover slips were flushed with an excess of ultrapure water. The cover slips were then soaked in a hot (70 - 80°C) bath of 30% hydrogen peroxide in 2.4 M HCl for 10 minutes as a second, polishing etching step. The HCl/peroxide mixture was similarly prepared by slow addition of the peroxide to avoid rapid boiling of the solution. The HCl/peroxide solution was then drained, and the cover slips were flushed with an excess of ultrapure water. The slides were then dried under a N_2 stream.

The dried RCA-cleaned cover slips were passivated by coupling of a PEG-silane layer to the glass surface. Briefly, a 5 mg/mL solution of mPEG-silane-5000 was prepared in anhydrous isopropanol, where both the isopropanol and mPEG-silane (which is oxygen-reactive) were handled under a pure N_2 atmosphere (using a Spilfyter "Hands-in-bag" artificial atmospheric chamber purchased from VWR International (Radnor, PA) to prevent contact with air). 1% v/v glacial acetic acid was added to catalyze the coupling reaction between the silane group and the $Si\text{-}OH^-$ groups on the etched glass surface. 50 µL drops of the PEG-silane solution were placed on one cover slip, and a second cover slip was placed over the first one to sandwich the PEG-silane liquid film between the two cover slips, spreading out the PEG-silane solution evenly over the entire slide surface. The back (un-passivated) sides of the slides were marked for easier identification of the passivated surface. The cover slip/PEG-silane 'sandwiches' were then dried at 70°C for ~30 minutes to remove the isopropanol. The slides were then separated from each

other by immersing the slide 'sandwiches' in ultrapure water and gently prying them apart underwater with tweezers. The passivated slides were then individually rinsed 2 – 3 times with ultrapure water and dried under a N_2 stream, before being stored in glass carafes under air prior to use. The passivated slides were used within 1 week of preparation.

Serial addition scheme for loading mAb samples onto wet-passivated slides

Due to the presence of 20 μL buffer present from DOPC passivation, it was necessary to add the labeled mAb sample to the imaging well using a serial addition scheme to minimize dilution. The mAb sample was added in a 4-step addition scheme to bring the final mAb concentration in the well to 95.83% of the original sample concentration. In this scheme, 20 μL of mAb sample was mixed into the imaging well by pipetting, and 20 μL of the mixed solution (out of the total 40 μL now in the well) was withdrawn. This step was repeated two more times, and in a final (4^{th}) addition, 40 μL of the original labeled sample was added. This scheme can alternatively be seen as serial dilution of the original buffer in the imaging well to 4.17% v/v of the final solution in the imaging well, with the remaining 95.83% of the solution volume corresponding to the original (undiluted) mAb sample. Due to the high viscosity of the mAb solutions, the viscous mAb solution had to be gently mixed with the non-viscous buffer by pipetting over several minutes until the solution in the well was homogenous.

Method development – FCS at high concentrations for mAbs with wet and dry passivation

To examine the influence of the refractive index (RI) on the confocal waist radius, ω_{xy} was determined from calibration measurements using 3 nM holo-transferrin (Tf) labeled with Atto-488 in solutions of either 50 mM $NaHCO_3$ (RI = 1.33) or 50 wt% glycerol in 50 mM $NaHCO_3$ (RI = 1.41) (loaded on dry-passivated slides). These two values cover the RI range from the lowest mAb concentration (10 mg/mL) in pure buffer (21:30 mM Na:OAc) to the highest concentration (250 mg/mL) in the most optically-dense co-solute solution (1 M Im). The solution RI was determined from the mAb and co-solute concentrations with previously-measured co-solute dn/dc values{Hung, 2019 #1750} and an assumed protein dn/dc of 0.185 mL/g{Minton, 2007 #212} as described previously.{Hung, 2019

#1750} The change in RI caused a shift in the Tf τ_D (Fig. S2, Table S1). The corresponding expected diffusion coefficients D_s were calculated from the literature value{Yajima, 1998 #1705} of $D_0 = 6.7*10^{-7}$ cm^2/s for Tf in water at 25°C and corrected for the measured solvent viscosities (Table S1) using the generalized Stokes-Einstein equation (Eqn. 8). The ACFs were measured in triplicate, and ω_{xy} was calculated from the measured τ_D and known D_s (Eqn. 7), resulting in ω_{xy} values of 432 ± 8.8 nm for RI = 1.33 and 421 ± 8.3 nm for RI = 1.41. Based on the small change, ω_{xy} was assumed to remain constant across the RI range relevant to the mAb diffusion measurements, and the average of the two ω_{xy} values (427 ± 6.1 nm) was used for all future calculations of D_s. ω_{xy} was re-measured each time the FCS optical path was adjusted, and that ω_{xy} value was used to determine D_s from τ_D values measured in the same microscopy session. While the ω_{xy} values changed modestly (ranging between 377 and 427 nm) between microscope calibrations, their effects on D_s cancel out. They cancel out because ω_{xy} is determined from the τ_D of a calibration probe transferrin (Tf) with the above known D_0 ($\omega_{xy} = \sqrt{4\tau_{D,Tf}D_0}$), such that mAb D_s depends on the ratio of τ_D between the Tf calibration probe and the mAb sample ($D_s = D_0 * (\tau_{D,Tf}/\tau_{D,mAb})$).

To ensure measurement of the diffusion of representative equilibrated mAb structures (monomer and possible oligomers) at high concentration, the labeled monomeric mAb was added to the mAb solution either at low concentration before ultrafiltration to ~200 mg/mL ("pre-spiked") or after ultrafiltration ("post-spiked"). These experiments were done on wet passivated slides. Both approaches were used to determine whether there were any time-dependent effects relating to exchange of labeled/unlabeled mAb between monomer and oligomer. In the "pre-spiked" case, the probe mAb undergoes exchange and self-association as it is concentrated from ~25 mg/mL to 200+ mg/mL. In the "post-spiked" case, it was not known if the monomeric probe had sufficient time to exchange into the oligomers in the viscous solution over a time scale of 10 – 15 minutes. However, an examination of the results for the two cases showed that there was no significant difference in terms of the ACF (Fig. 1) or the fit parameters G(0), τ_D (Ds) or α (Table 1), suggesting that exchange of the labeled mAb between

monomer and oligomer reached equilibrium in the time frame between probe addition and FCS measurements (~10 minutes). This result is consistent with the short lifetimes of dynamic protein clusters, which have been suggested to be on the order of 25 ns.{Porcar, 2010 #1994} Another possibility is that the fraction of reversible oligomers may be too low to be measureable by FCS. Thus, for the remaining experiments, the mAb probe was added to the formulated samples at high concentration for simplicity as well as to minimize the amount of time the labeled mAb spends in the liquid state to minimize risk of dye hydrolysis.

The G(0) value has been shown to decrease with increasing crowder (protein, polymer, vesicles, etc.) concentration{Engelke, 2009 #1404} to very small values (un-normalized << 2 or normalized << 1),{Reitan, 2008 #1402}{Starr, 2002 #1413} which may potentially lead to poor signal-to-noise ratios. Based on Eqn. 6, the low G(0) may be caused by the detection of large number of fluorophores N in the confocal volume. Interestingly, G(0) decreased with increasing mAb concentration, as seen in Fig. S4a and Table S2 for the 250 mM PheOMe system, as well as in Table S3 for additional formulations from 60 to 250 mg/mL, despite the fact that the labeled mAb concentration was fixed at 1 nM for all samples. N (and therefore G(0)) should in theory remain fixed for a given labeled mAb concentration. This unusual increase in apparent N has instead been attributed in part to an enlargement in the effective confocal volume (molecular detection function, "MDF") due to multiple scattering of the excitation light by the concentrated surrounding unlabeled protein,{Engelke, 2009 #1404} resulting in illumination of a larger volume than is expected. This effect is still not fully understood, but simulations suggest that this distortion of the MDF is minimized or eliminated by working at focal depths less than 50 μm from the cover slip.{Engelke, 2009 #1404} Similarly, RI mismatch is known to distort the MDF under certain conditions,{Müller, 2008 #1599}{Wang, 2012 #1608} but these effects were also shown from simulations to be minimized at < 20 μm from the cover slip.{Wang, 2012 #1608}{Müller, 2008 #1599} To optimize G(0) and minimize the MDF distortion effects, the ACFs and corresponding G(0) of mAb2 at 200 mg/mL in 1 M Im(HCl) were measured as a function of focal depth from the cover slip between 3 and 20 μm (precisely controlled using the piezoelectric stage). As can be seen in Fig. 2, G(0) increased

with decreasing focal depth, with negligible effects on the corresponding τ_D and α within measurement error. Given that both G(0) is maximized and MDF distortion effects are minimized closest to the cover slip, the focal depth was fixed at 3 μm from the cover slip for subsequent measurements. The ACFs G(τ) were fit in the un-normalized form (Eqn. 6 and Eqn. 9). However, to facilitate easier visual comparison of ACFs between mAb concentrations and formulations given the wide range of G(0)'s, they are shown in the Supporting Information as normalized G(τ)'s where the normalized G(0) = 1. Similarly, the normalized G(τ) → 0 as τ → ∞, since the un-normalized G(τ) → 1 as τ → ∞.

$$Normalized\ G(\tau) = \frac{G(\tau)-1}{G(0)-1} \quad (14)$$

In Eqn. 14, G(0) is the initial value of the un-normalized G(τ), and is reported (un-normalized) for all mAb concentrations and formulations in Table S3.

To ensure reproducible, meaningful measurements of the mAb diffusion at high concentration and viscosity, the sample loading technique was refined in conjunction with the slide passivation strategy to eliminate sample heterogeneity introduced by the loading technique. In the wet passivation technique{Busch, 2015 #1713}{Houser, 2016 #1712}{Snead, 2017 #1711} as well as for the method development experiments described in previous sections, the mAb sample was added to the imaging well which already contained a thin layer of fluid. A serial addition/mixing scheme was utilized to bring the final mAb concentration in the well back to ~96% of the initial sample concentration. For relatively non-viscous samples such as 250 mM Arg.HCl (~20 cP at 200 mg/mL), the sample was easy to mix evenly, resulting in good reproducibility of the ACF between replicate measurements. However, for viscous samples such as 250 mM NaCl (60 – 70 cP at 200 mg/mL), the confined geometry of the sample well and the high viscosity resulted in uneven mixing of the sample and poorer reproducibility between replicate ACF measurements (not shown). In contrast, the dry passivation technique demonstrated superior reproducibility even for viscous samples (Fig. 3a), since the mAb sample is loaded directly onto the dry, passivated slide without any mixing or sample dilution needed, resulting in consistent mAb

concentrations and homogenous samples in the imaging well. The dry-passivated slides were therefore used for the remaining samples examined in this study.

Chi square minimization for ACF fitting

The raw ACFs obtained from FCS were fit to the different mathematical models (Eqn. 6 and 9) by minimizing χ^2 (Eqn. S1):

$$\chi^2 = \sum \left(\frac{G^{theo}(\tau_i) - G^{expt}(\tau_i)}{\sigma_i} \right)^2 \tag{S1}$$

Where $G^{theo}(\tau_i)$ is the correlation value calculated from the model, $G^{expt}(\tau_i)$ is the measured correlation value, and σ_i is the standard deviation of each measurement. Since the uncertainty in each measurement is not easily obtainable from the FCS instrument,[6] an algorithm was developed to approximate this from the noise in the neighboring points. For a given delay time, τ_i, different values of $G(\tau_i)$ were calculated from all possible linear interpolations over the range from $[\tau_{i-1}:\tau_{i-5}]$ to $[\tau_{i+1}:\tau_{i+5}]$ (Eqn. S2). The average and standard deviation of $G^{expt}(\tau_i)$ were given by the average and standard deviation of the set of $G_{j,k}(\tau_i)$ values, which contains 25 interpolations as well as the measured point (Eqn. S3 and S4).

$$G_{j,k}(\tau_i) = G^{expt}(\tau_{i-j}) + \frac{G^{expt}(\tau_{i+k}) - G^{expt}(\tau_{i-j})}{\tau_{i+k} - \tau_{i-j}} (\tau_i - \tau_{i-j}) \begin{cases} 1 \le j \le 5 \\ 1 \le k \le 5 \end{cases} \tag{S2}$$

$$\bar{G}(\tau_i) = \frac{1}{26} \left(G^{expt}(\tau_i) + \sum_{j=1}^{5} \sum_{k=1}^{5} G_{j,k}(\tau_i) \right) \tag{S3}$$

$$\sigma_i = \sqrt{\frac{1}{26} \left(\left(G^{expt}(\tau_i) - \bar{G}(\tau_i) \right)^2 + \sum_{j=1}^{5} \sum_{k=1}^{5} \left(G_{j,k}(\tau_i) - \bar{G}(\tau_i) \right)^2 \right)} \tag{S4}$$

Therefore, if there are large fluctuations in the measured correlation values around a certain point, the interpolated correlation values will also fluctuate, resulting in a large standard deviation. This method was validated using measured ACFs, shown in Fig. S17a and S17b, where the calculated standard deviation correctly approximated the noise in the data. χ^2 minimization also improved the fits of noisier samples

significantly compared to the standard residual minimization. As shown in Fig. S17c, the fitted ACF obtained using standard residuals shows significant systematic over- and under-fitting, whereas the χ^2 fit follows the experimental curve without any systematic deviations from the data. This is because each residual in the χ^2 fit is weighted by its standard deviation, so the regions of the ACF with large noise have a smaller influence on the overall goodness of fit.

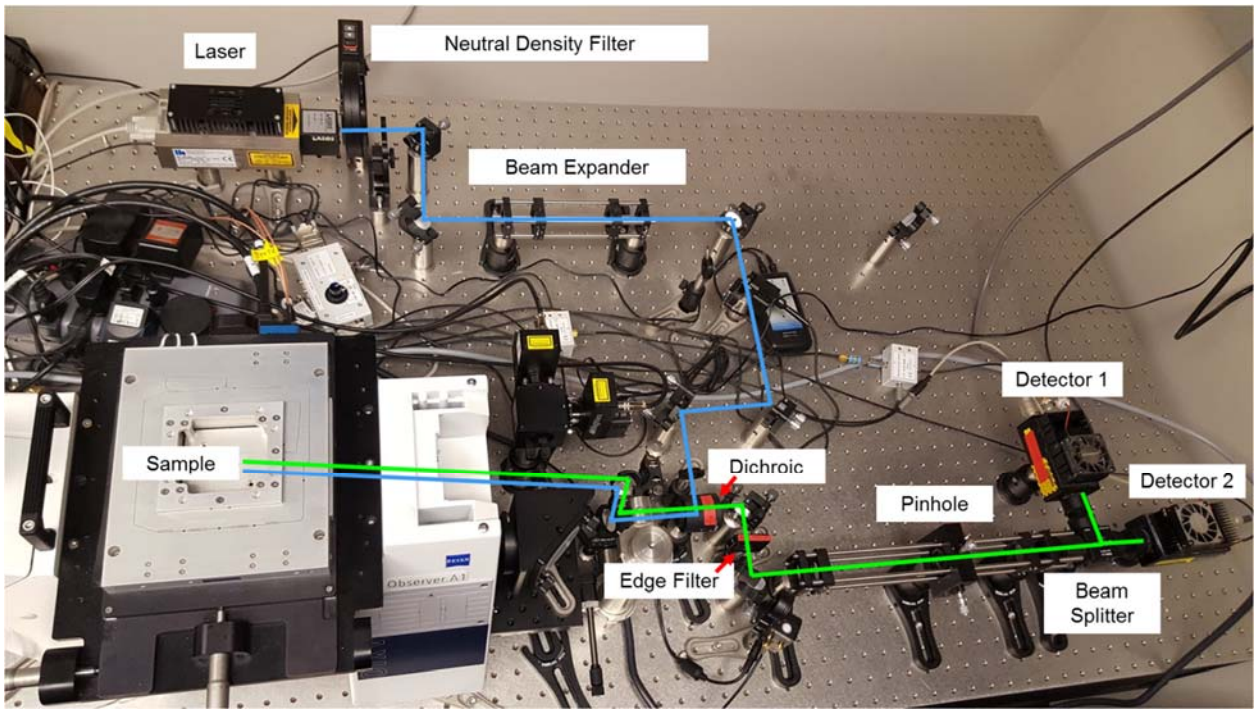

Figure S1. Optical path and setup of the home-built FCS instrument.

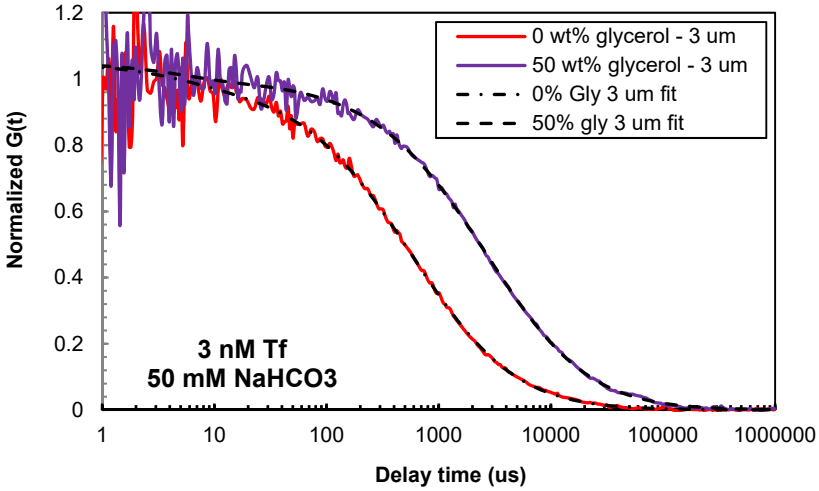

Figure S2. Effect of the solution refractive index (RI) on the normalized ACF of Atto488-labeled holo-transferrin in 50 mM NaHCO3 (pH 8.3). The RI were chosen to replicate the solution refractive index at the lowest (~1 mg/mL) and highest (~250 mg/mL) mAb concentrations. The transferrin ACFs were used to calibrate the confocal volume waist radius (Table S1) and determine if there were RI effects on the waist radius across the range of RI values relevant to the high concentration mAb FCS measurements. The samples were loaded on dry-passivated slides.

Table S1. Dependence of the calibrated confocal volume waist radius on the solution refractive index (RI). The waist radius ω_{xy} was calculated from τ_D obtained from the 3D anomalous diffusion fits of the ACF of Atto488-labeled holo-transferrin in 0 and 50 wt% glycerol (Fig. S2) using the known value[7] of D_0 of $6.7*10^{-7}$ cm^2/s for holo-transferrin at 25°C in water, corrected for the solvent viscosity η_0. The samples were loaded on dry-passivated slides. ω_{xy} was taken as the average value 427 ± 6.1 nm.

Focal depth (μm)	Glycerol conc (wt %)	Solution RI	η_0 (cP)	τ_D (μs)	α	Calc ω_{xy} from lit value of Tf D_0 (nm)
3	0	1.33	0.89	696 ± 28	0.81 ± 0.01	432 ± 8.8
3	50	1.41	4.97	3284 ± 130	0.84 ± 0.01	421 ± 8.3

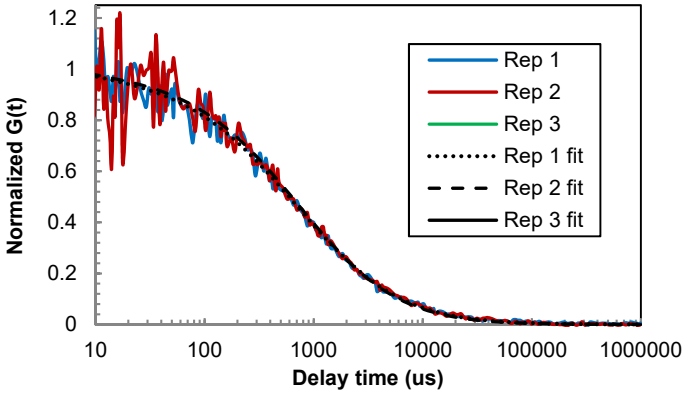

Figure S3. Normalized ACF of 1 nM Atto488-labeled mAb2 in buffer (21:30 mM Na:OAc, pH 5) measured in triplicate using wet-passivated slides. The ACF was fit to the 3D anomalous diffusion model (α = 0.81 ± 0.03), and

the fitted τ_D of 846 ± 25 µs was used as the monomer diffusion time for calculating D_s/D_0 of mAb2 at high concentration in 250 mM PheOMe(HCl) (Fig. S4)

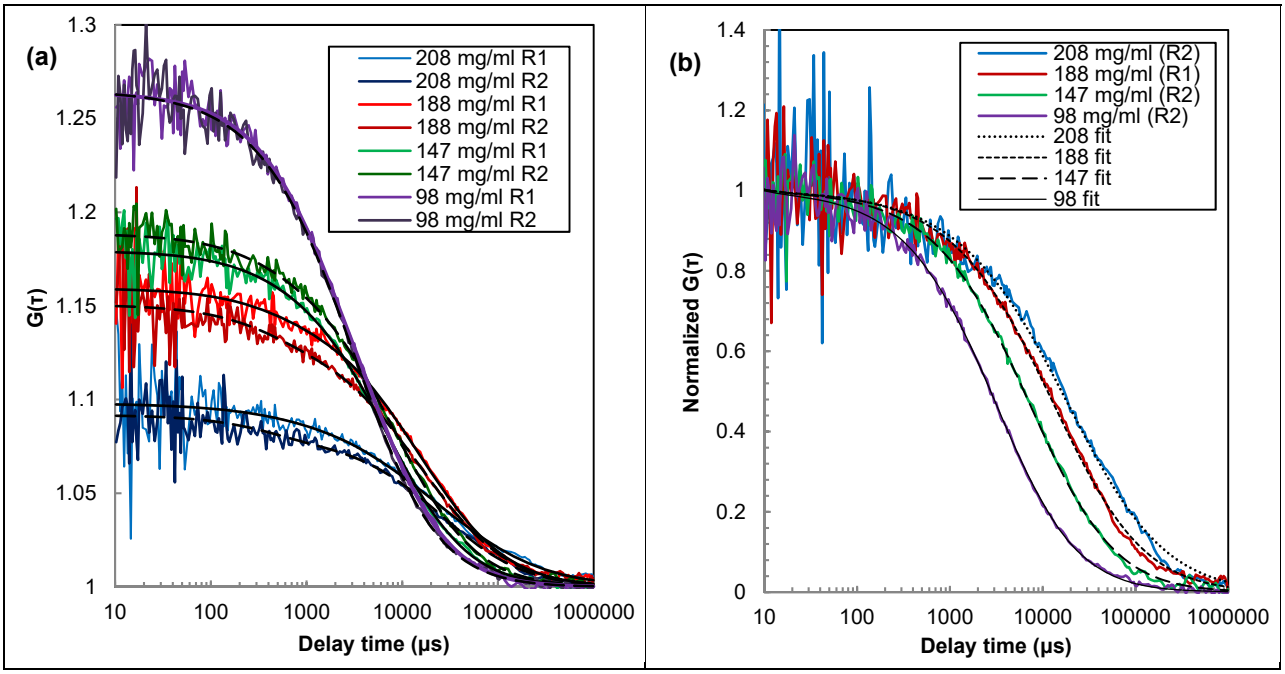

Figure S4. Concentration dependence of the **(a)** non-normalized and **(b)** normalized FCS ACFs of mAb2 in 250 mM PheOMe(HCl) at pH 5.5. Samples were loaded on wet-passivated slides. The corresponding τ_D, α and D_s/D_0 fit from the ACFs are reported in Table S2. Smoothed solid/dashed black curves show fits of the ACFs to the anomalous 3D diffusion model.

Table S2. Concentration dependence of the diffusivity D_s/D_0 and corresponding anomaly coefficient α of mAb2 in 250 mM PheOMe(HCl) at pH 5.5 fit from the ACFs in Fig. S4 to the anomalous 3D diffusion model. D_s/D_0 was calculated from the ratio of the monomer $\tau_{D,0}$ of 846 µm (Fig. S3) to τ_D.

mAb conc (mg/mL)	G(0) (Not normalized)	τ_D (µs)	D_s/D_0	α
98	1.26	3872 ± 195	0.22 ± 0.01	0.85 ± 0.01
147	1.18	8211 ± 666	0.10 ± 0.01	0.83 ± 0.03
188	1.15	15262 ± 918	0.06 ± 0.00	0.74 ± 0.04
208	1.09	23640 ± 875	0.04 ± 0.00	0.71 ± 0.00

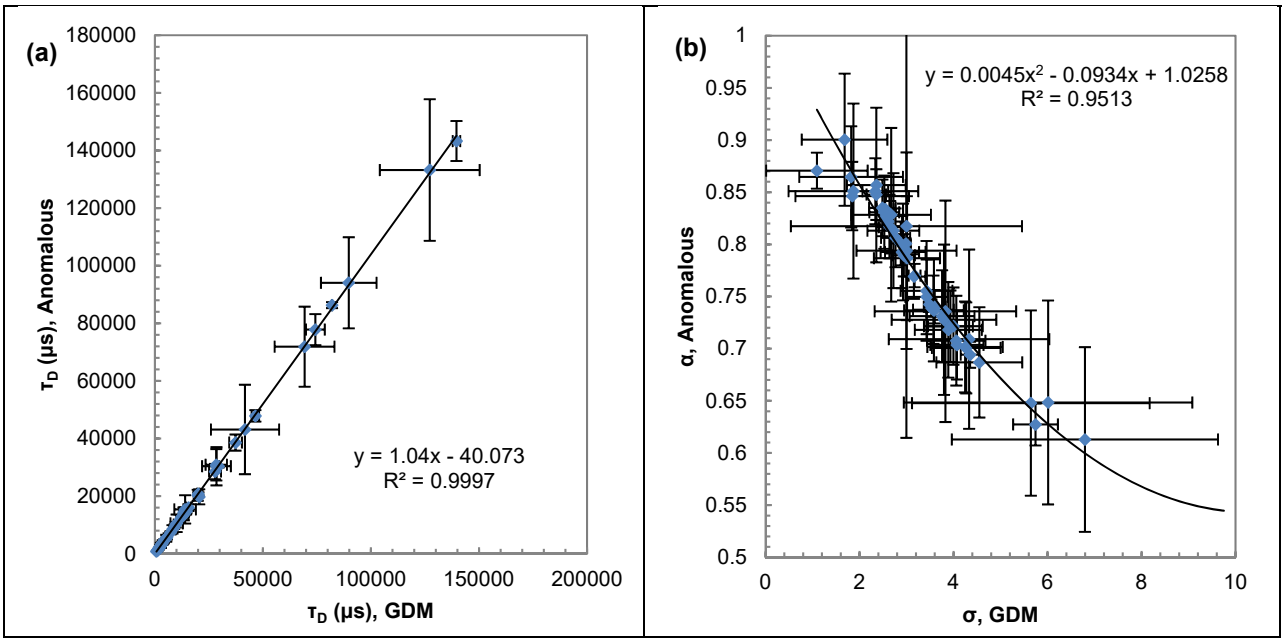

Figure S5. Correspondence of **(a)** the diffusion cross-over time τ_D and **(b)** anomaly coefficient α or standard deviation σ between the 3D anomalous diffusion and GDM models fits, respectively, of the mAb2 FCS ACFs across all tested mAb concentrations and co-solute formulations. All samples were measured in triplicate using dry-passivated slides at a focal depth of 3 μm.

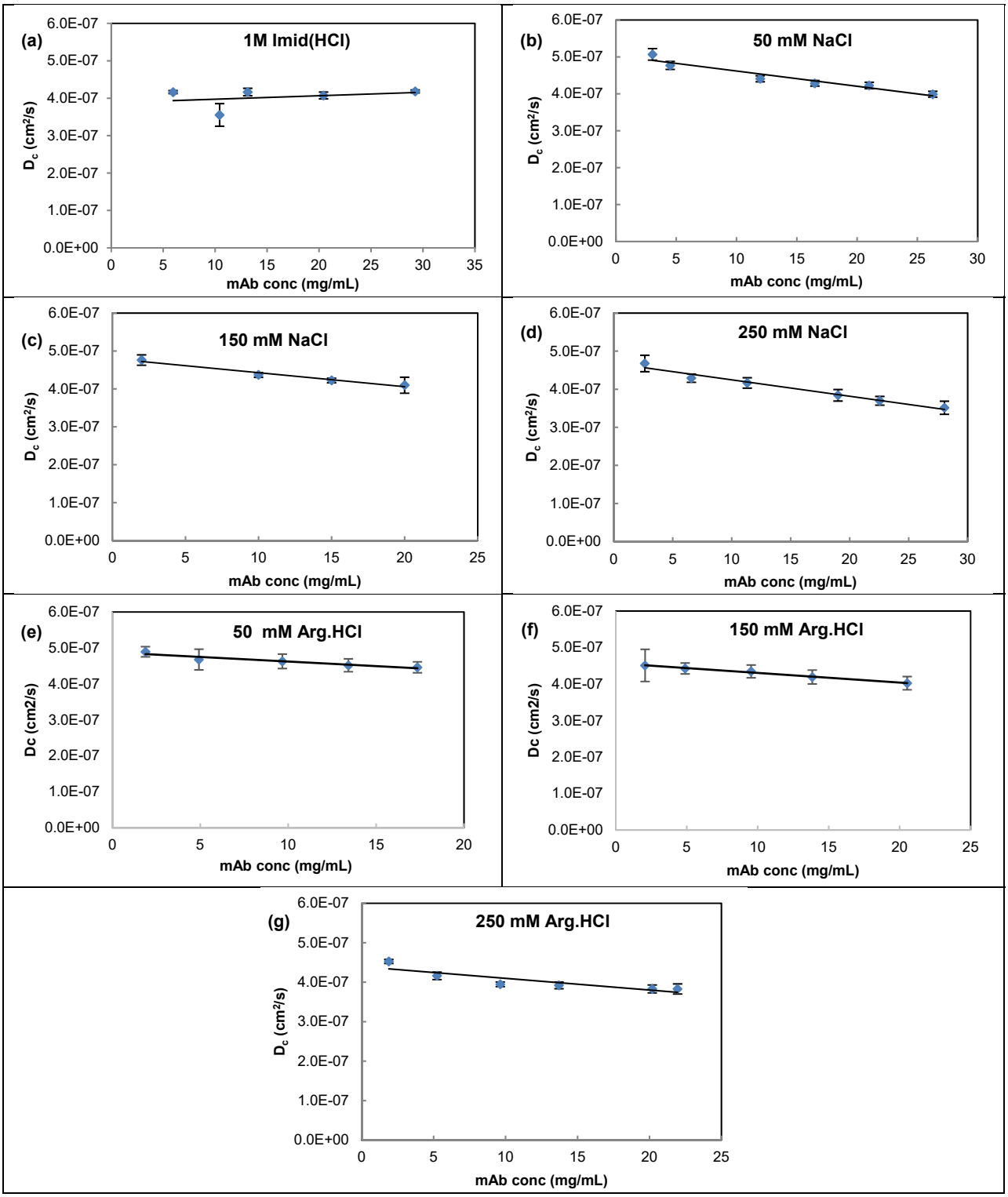

Figure S6. Dependence of D_c ($\sim D_z$) of mAb2 from 2 – 20 mg/mL in different co-solute formulations as measured by DLS. D_0 was obtained from linear fits of D_c vs concentration to Eqn. 5. The formulations are **(a)** 1 M Im(HCl) titrated to pH 5.5, **(b)** 50 mM NaCl, **(c)** 150 mM NaCl, **(d)** 250 mM NaCl, **(e)** 50 mM Arg.HCl, **(f)** 150 mM Arg.HCl, **(g)** 250 mM Arg.HCl.

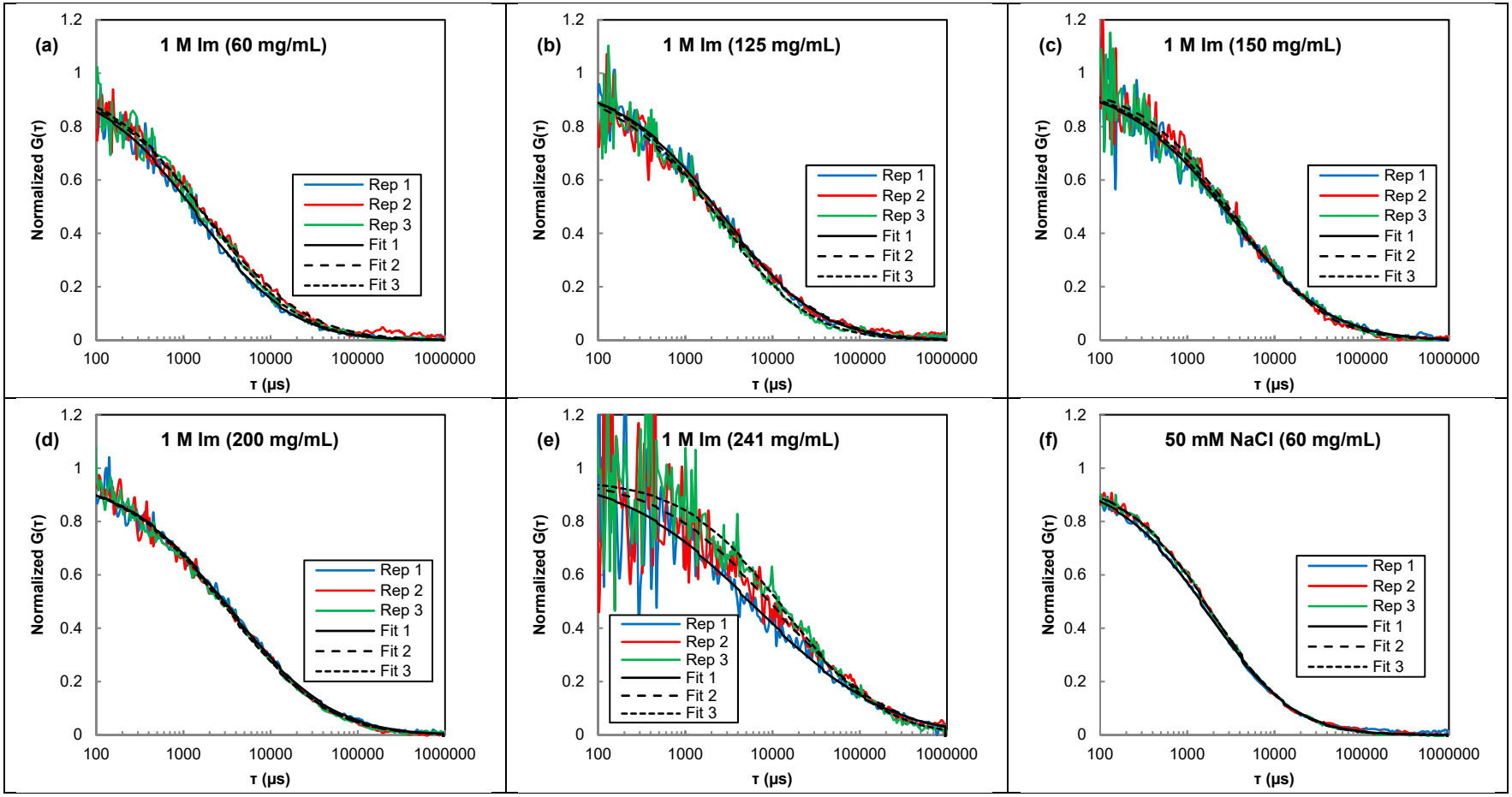
(a)
1 M Im (60 mg/mL)
(b)
1 M Im (125 mg/mL)
(c)
1 M Im (150 mg/mL)
(d)
1 M Im (200 mg/mL)
(e)
1 M Im (241 mg/mL)
(f)
50 mM NaCl (60 mg/mL)
Normalized G(τ)
τ (μs)
Rep 1
Rep 2
Rep 3
Fit 1
Fit 2
Fit 3

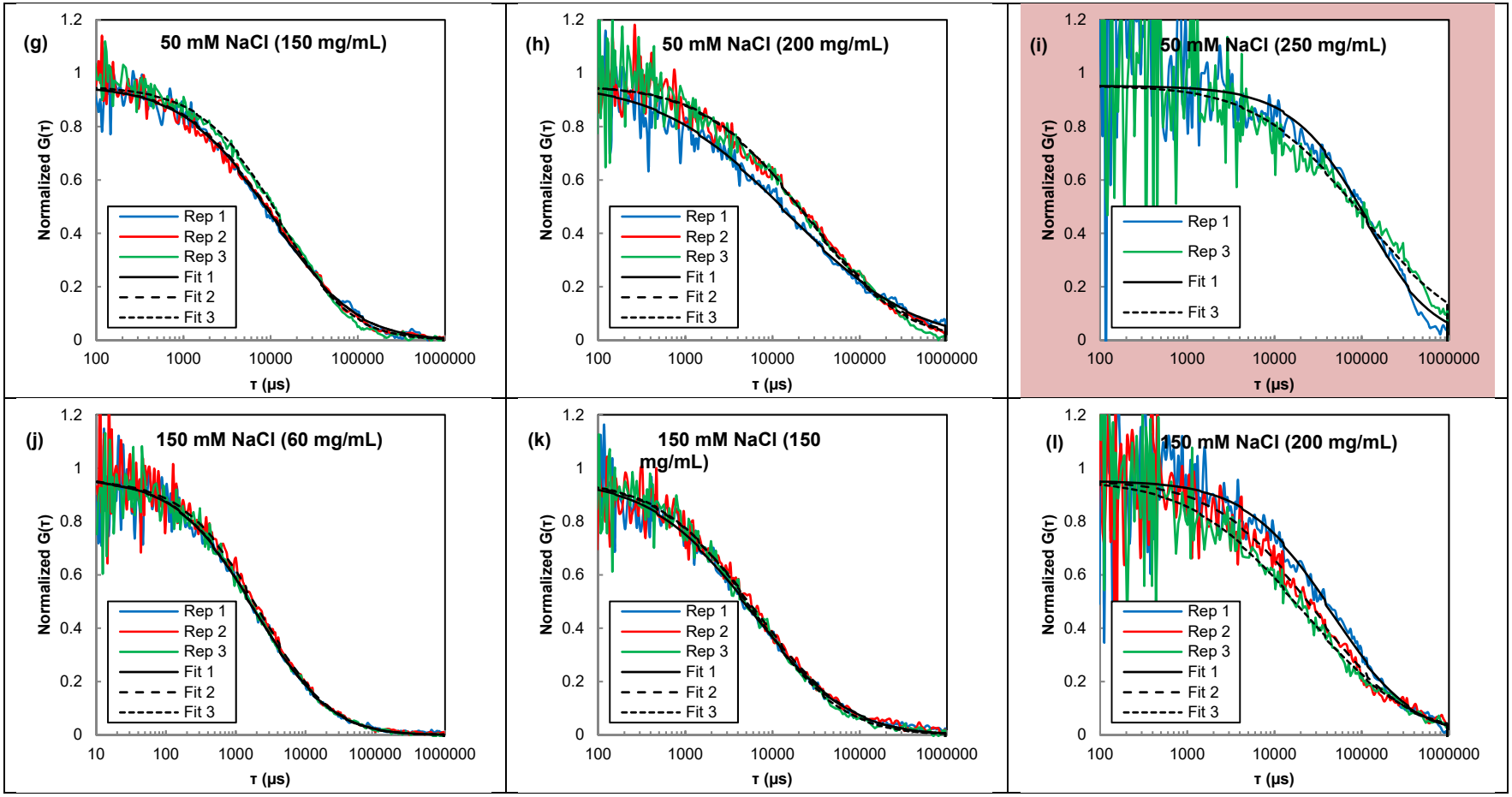
(g)
50 mM NaCl (150 mg/mL)
(h)
50 mM NaCl (200 mg/mL)
(i)
50 mM NaCl (250 mg/mL)
(j)
150 mM NaCl (60 mg/mL)
(k)
150 mM NaCl (150 mg/mL)
(l)
150 mM NaCl (200 mg/mL)
Normalized G(τ)
τ (µs)
Rep 1
Rep 2
Rep 3
Fit 1
Fit 2
Fit 3

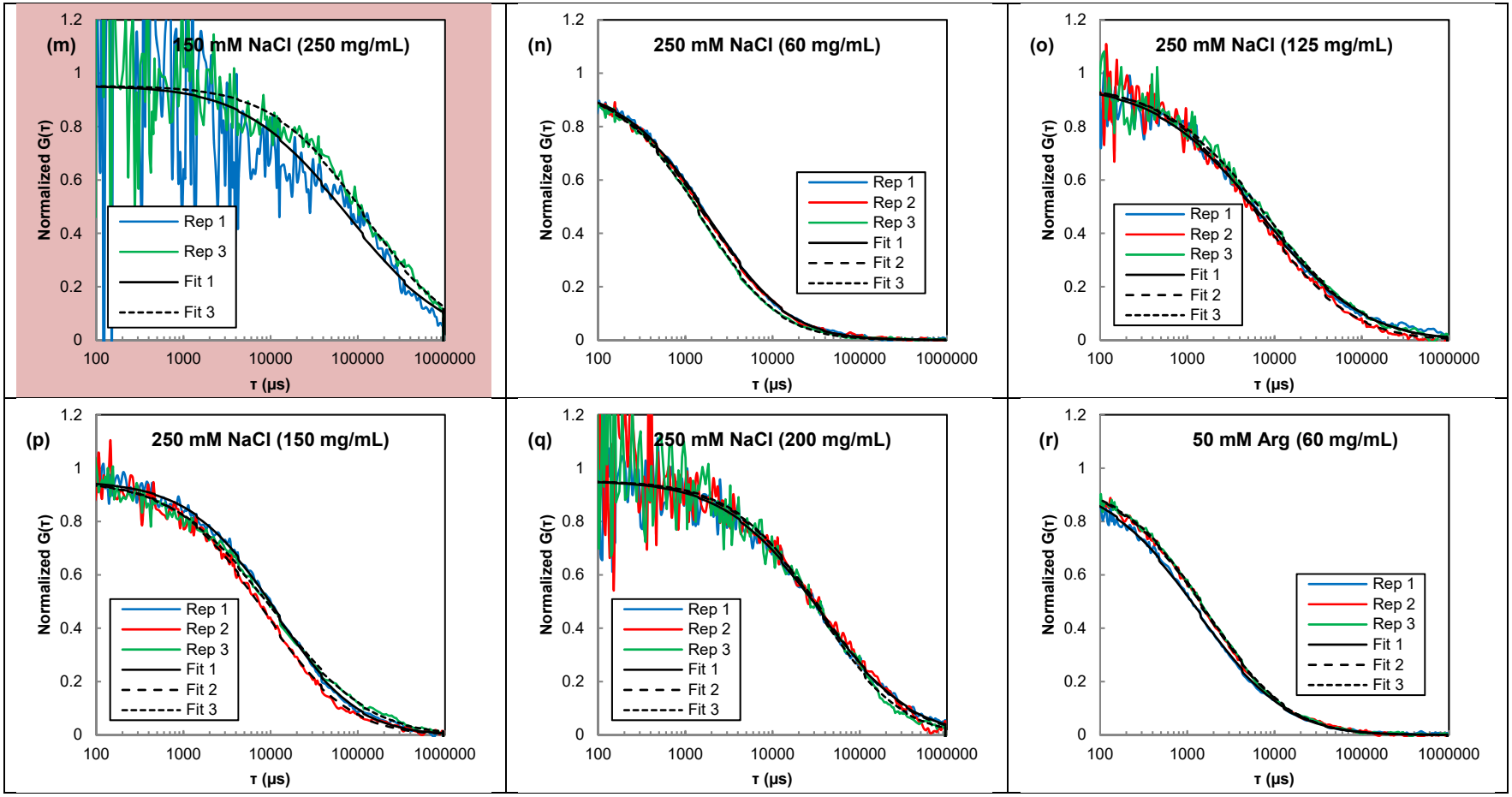
(m)
150 mM NaCl (250 mg/mL)
(n)
250 mM NaCl (60 mg/mL)
(o)
250 mM NaCl (125 mg/mL)
(p)
250 mM NaCl (150 mg/mL)
(q)
250 mM NaCl (200 mg/mL)
(r)
50 mM Arg (60 mg/mL)
Normalized G(τ)
τ (µs)
Rep 1
Rep 2
Rep 3
Fit 1
Fit 2
Fit 3

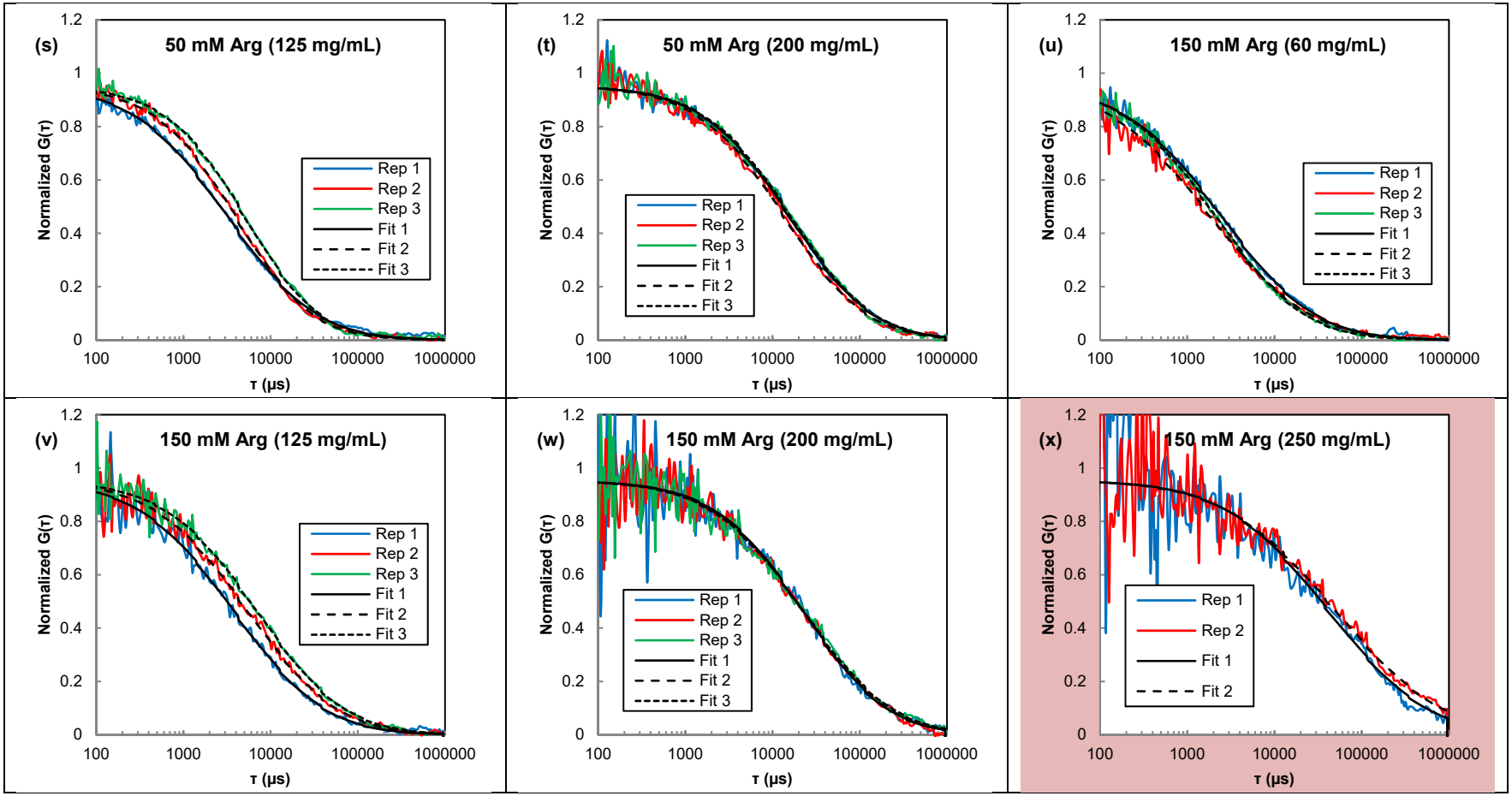
(s)
50 mM Arg (125 mg/mL)
(t)
50 mM Arg (200 mg/mL)
(u)
150 mM Arg (60 mg/mL)
(v)
150 mM Arg (125 mg/mL)
(w)
150 mM Arg (200 mg/mL)
(x)
150 mM Arg (250 mg/mL)
Normalized G(τ)
τ (µs)
Rep 1
Rep 2
Rep 3
Fit 1
Fit 2
Fit 3

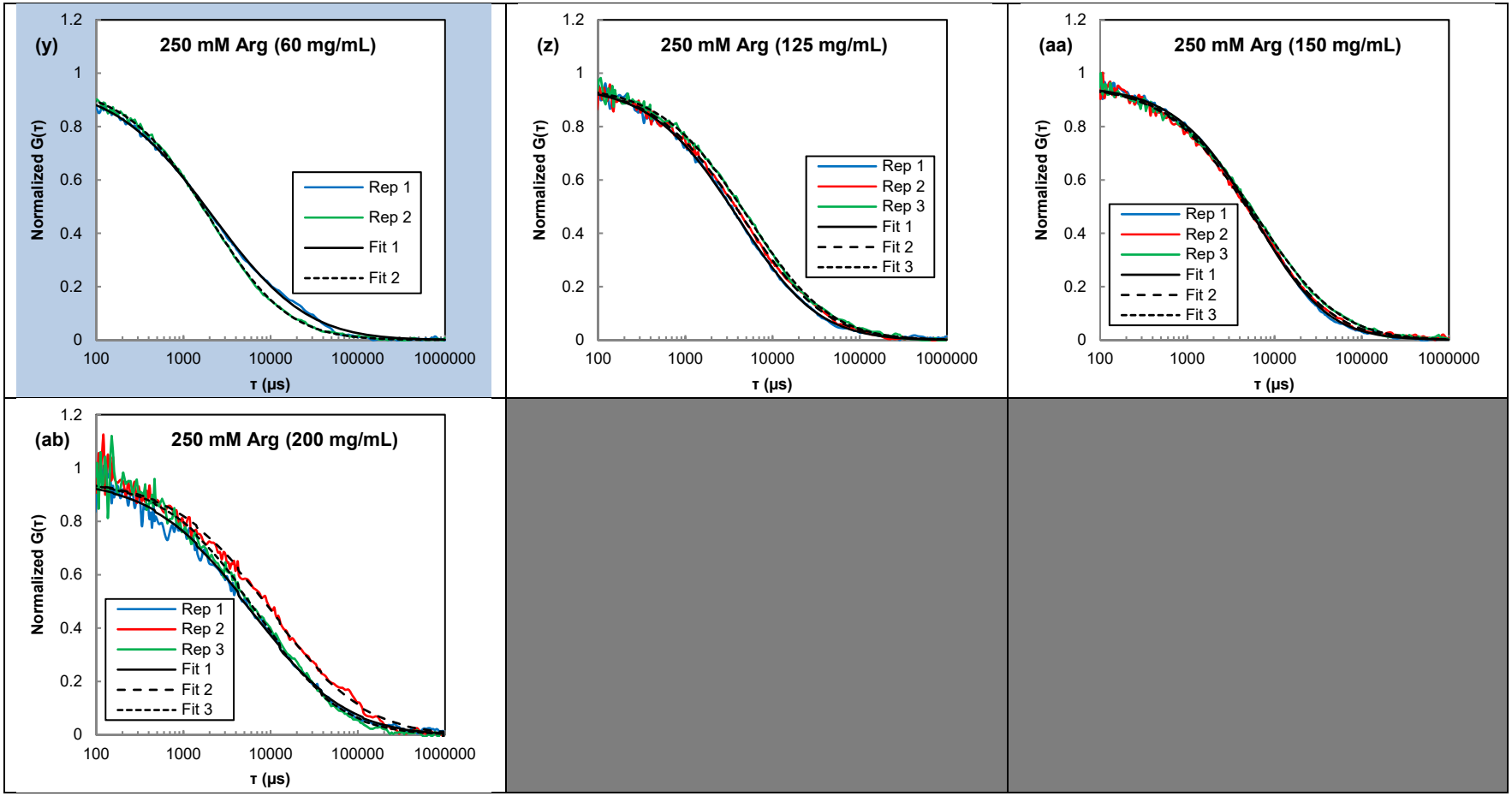

Figure S7. Normalized autocorrelation function (ACF) replicates of mAb2 for all co-solute systems at 60, 125, 150, 200, ~225 and ~250 mg/mL. The ACFs were normalized by the G(0) values of the raw ACFs (Table S3). ACFs are shown for 1 M Im(HCl) at **(a)** 60 mg/mL, **(b)** 125 mg/mL, **(c)** 150 mg/mL, **(d)** 200 mg/mL, **(e)** 241 mg/mL; 50 mM NaCl at **(f)** 60 mg/mL, **(g)** 150 mg/mL, **(h)** 200 mg/mL, **(i)** 250 mg/mL; 150 mM NaCl at **(j)** 60 mg/mL, **(k)** 150 mg/mL, **(l)** 200 mg/mL, **(m)** 250 mg/mL; 250 mM NaCl at **(n)** 60 mg/mL, **(o)** 125 mg/mL, **(p)** 150 mg/mL, **(q)** 200 mg/mL; 50 mM Arg.HCl at **(r)** 60 mg/mL, **(s)** 125 mg/mL, **(t)** 200 mg/mL; 150 mM Arg.HCl at **(u)** 60 mg/mL, **(v)** 125 mg/mL, **(w)** 200 mg/mL, **(x)** 250 mg/mL; 250 mM Arg.HCl at **(y)** 60 mg/mL, **(z)** 125 mg/mL, **(aa)** 150 mg/mL and **(ab)** 200 mg/mL

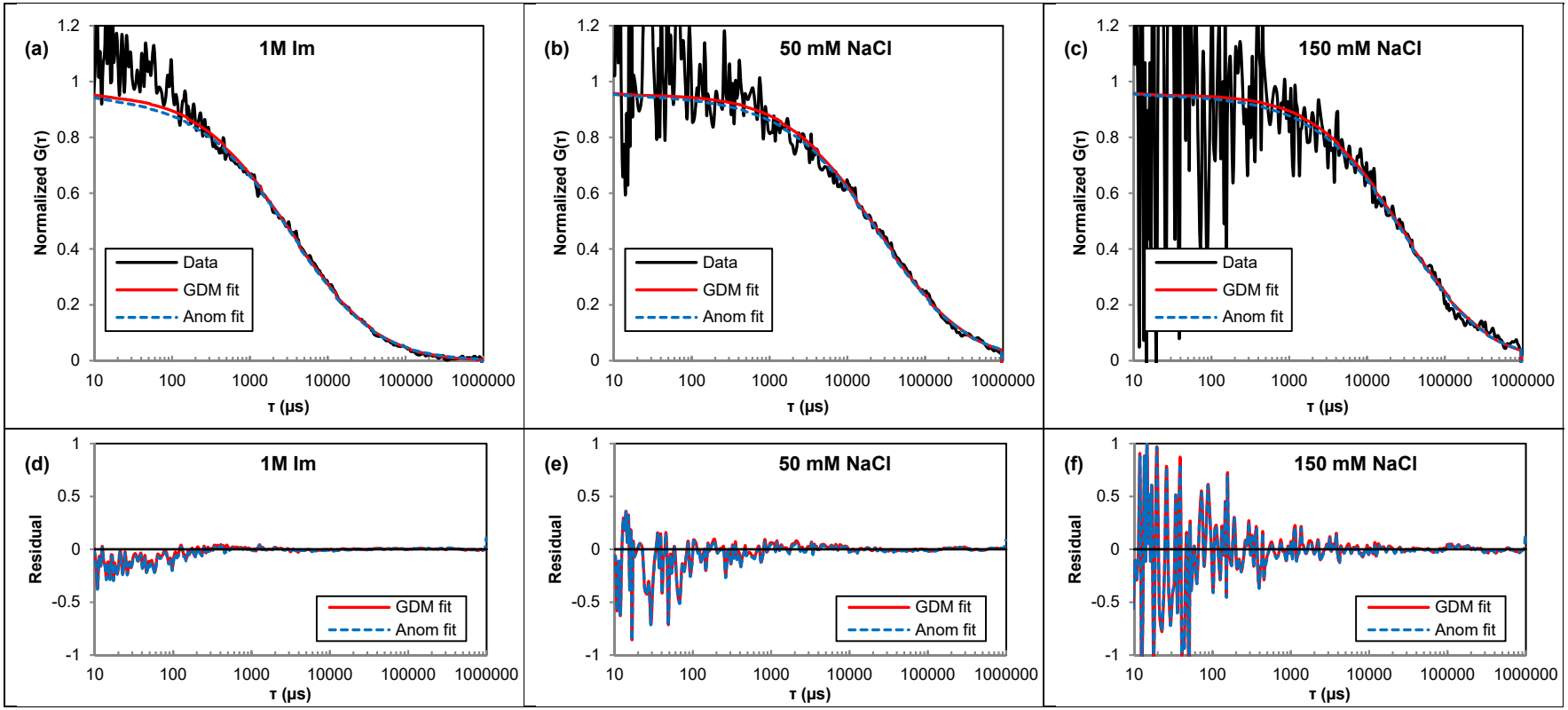
(a)
1M Im
(b)
50 mM NaCl
(c)
150 mM NaCl
Normalized G(τ)
Data
GDM fit
Anom fit
τ (μs)
(d)
1M Im
(e)
50 mM NaCl
(f)
150 mM NaCl
Residual
GDM fit
Anom fit
τ (μs)

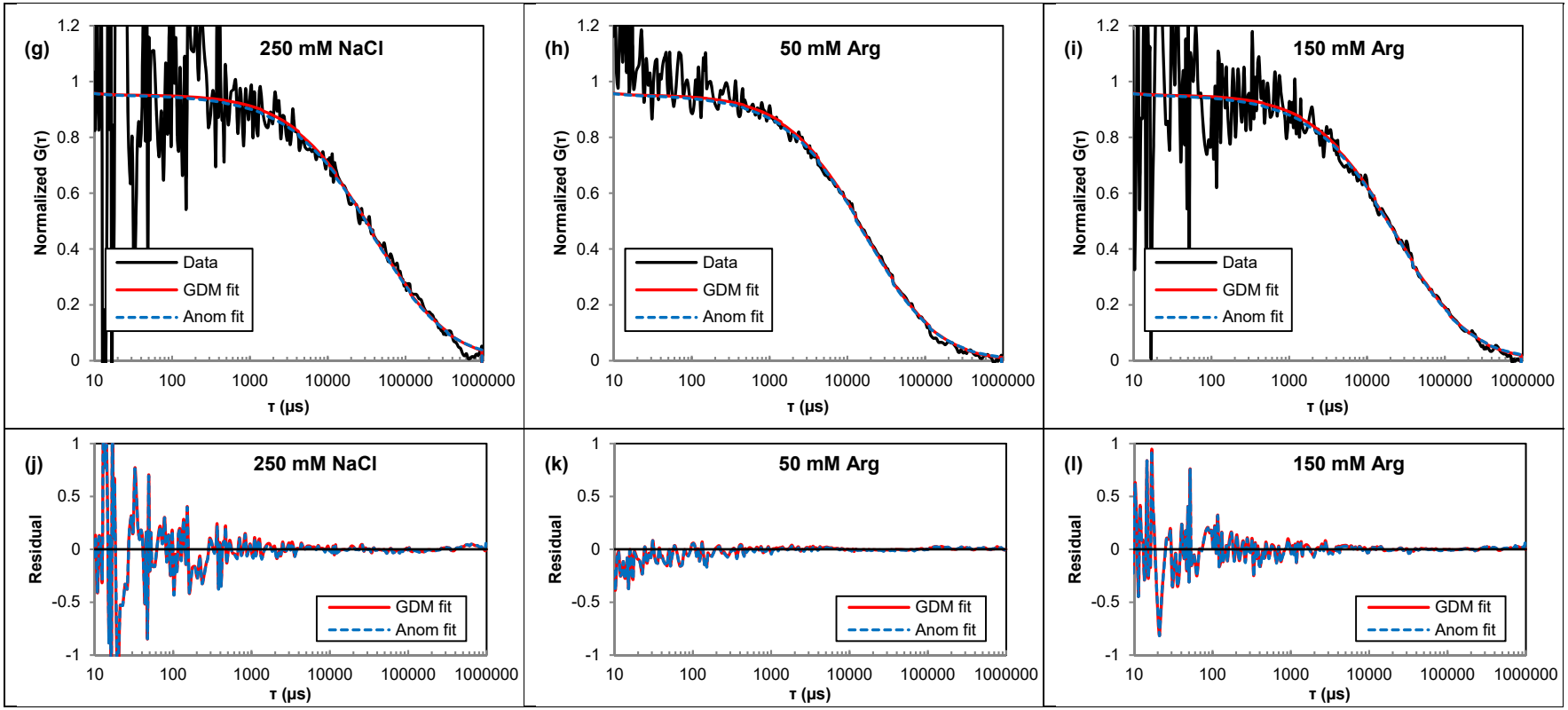
(g)
250 mM NaCl
Normalized G(τ)
Data
GDM fit
Anom fit
τ (μs)
(h)
50 mM Arg
Normalized G(τ)
Data
GDM fit
Anom fit
τ (μs)
(i)
150 mM Arg
Normalized G(τ)
Data
GDM fit
Anom fit
τ (μs)
(j)
250 mM NaCl
Residual
GDM fit
Anom fit
τ (μs)
(k)
50 mM Arg
Residual
GDM fit
Anom fit
τ (μs)
(l)
150 mM Arg
Residual
GDM fit
Anom fit
τ (μs)

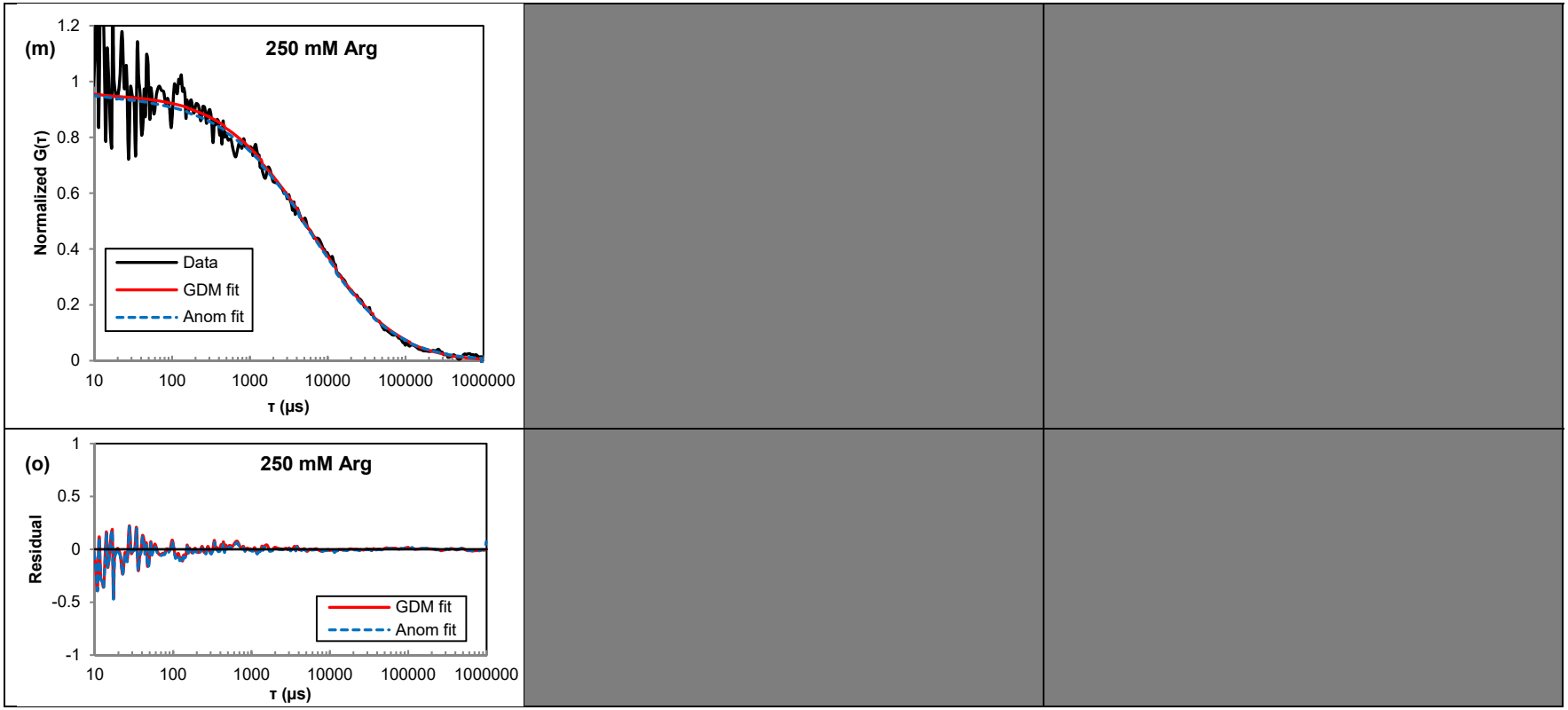

Figure S8. Comparison of fits (with residuals) of the 200 mg/mL mAb2 ACFs to the Gaussian distribution model (GDM) and anomalous 3D diffusion model (Anom). The fits and residuals are shown respectively for **(a, d)** 1M Im(HCl) at pH 5.5, **(b, e)** 50 mM NaCl, **(c, f)** 150 mM NaCl, **(g, j)** 250 mM NaCl, **(h, k)** 50 mM Arg.HCl, **(i, l)** 150 mM Arg.HCl, **(m, o)** 250 mM Arg.HCl.

Table S3. Average G(0) of the un-normalized ACFs in Fig. S7. The G(0) values were calculated from the average *N* obtained from fits of the un-normalized ACFs (measured in triplicate) to the 3D anomalous diffusion model (Eqn. 6). The measurements were made with dry-passivated slides.

	Un-normalized G(0)					
Formulation	**60**	**125**	**150**	**200**	**225**	**250**
50 mM NaCl	1.93 ± 0.12		1.3 ± 0.03	1.15 ± 0.02		1.05 ± 0.01
150 mM NaCl	1.39 ± 0.02		1.14 ± 0.03	1.10 ± 0.00		1.05 ± 0.04
250 mM NaCl	2.56 ± 0.38	1.17 ± 0.04	1.36 ± 0.06	1.11 ± 0.02	1.09 ± 0.01	
50 mM Arg.HCl	1.87 ± 0.10	1.82 ± 0.21		1.32 ± 0.02		
150 mM Arg.HCl	1.27 ± 0.02	1.21 ± 0.07		1.11 ± 0.01		1.06 ± 0.01
250 mM Arg.HCl	1.88 ± 0.15	1.31 ± 0.04	1.36 ± 0.04	1.20 ± 0.03	1.08 ± 0	1.04 ± 0.00
1 M Im(HCl)	1.12 ± 0.01	1.14 ± 0.03	1.09 ± 0	1.14 ± 0.00		1.02 ± 0.00

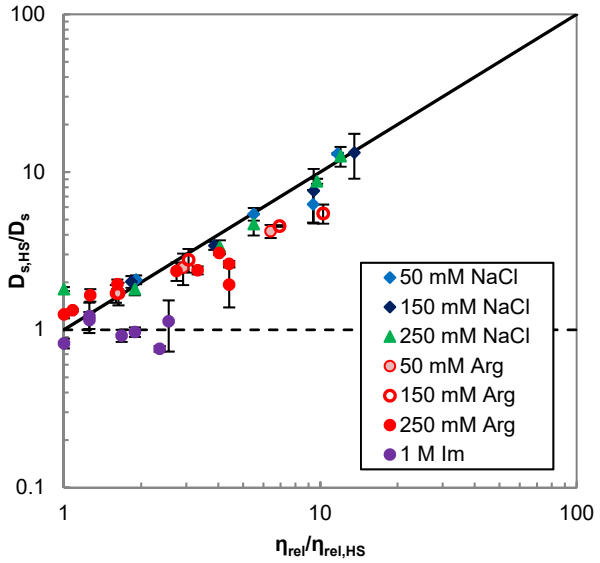

Figure S9. Dependence of the hard-sphere normalized self-diffusion coefficient $D_{s,HS}/D_s$ of mAb2 on the solution relative viscosity (normalized by the hard sphere viscosity at the same concentration) in different co-solute formulations. $D_{s,HS}/D_0$ and $\eta_{rel,HS}$ were calculated following Roos et al.[9] and the Ross-Minton equation (Eqn. 4) respectively for each point at the same corresponding mAb concentration (i.e. volume fraction φ), where the concentration was converted to φ using the average partial specific volume of mAb2 determined from fits of the mAb static light scattering[4] to the IHS model.[10] The mAb concentration groups and the corresponding normalizing HS values $D_0/D_{,HS}$ are shown in Fig. S11. The viscosities were calculated from the Ross-Minton equation (Eqn. 4) with the fit parameters from Table 2.

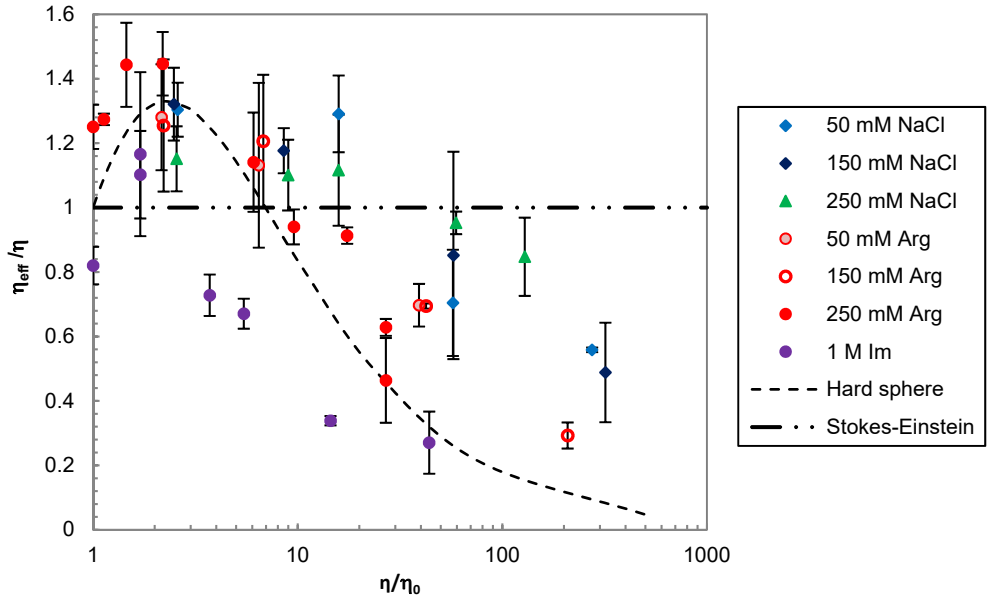

Figure S10. Dependence of the deviation of the microviscosity from the macroviscosity as a function of macroscopic viscosity and co-solute formulations. Measurements were done in triplicate on dry-passivated glass slides at a focal depth of 3 μm. The viscosities were calculated from the Ross-Minton equation (Eqn. 4) with the fit parameters from Table 2.

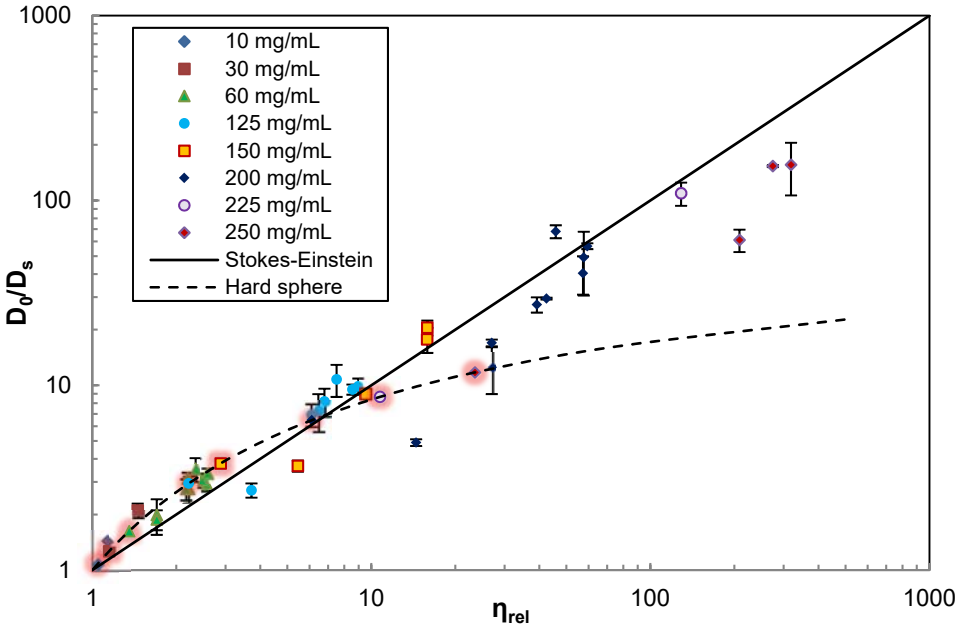

Figure S11. Dependence of the self-diffusion retardation factor D_0/D_s on the solution relative viscosity η_{rel}, grouped by the mAb concentration.

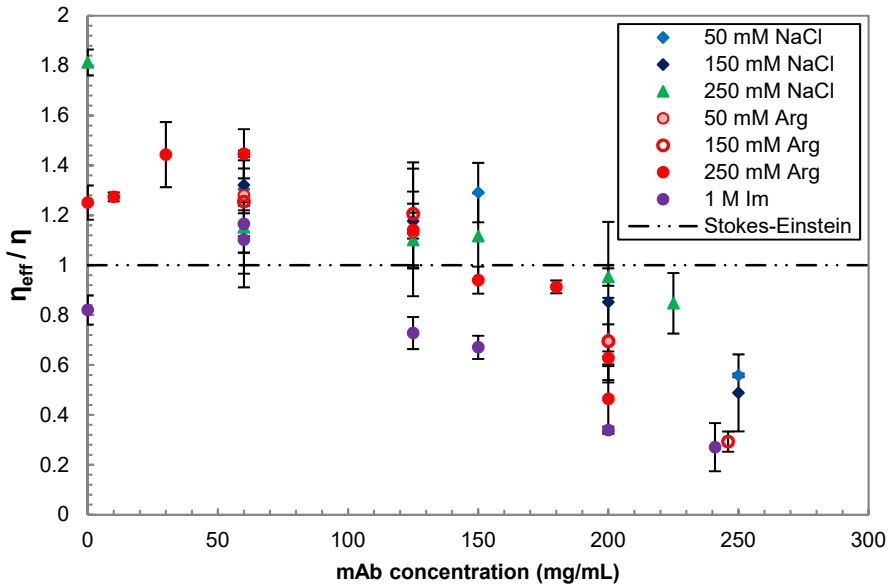

Figure S12. Concentration dependence of the effective viscosity (microviscosity) relative to the macroviscosity (η_{eff}/η) of mAb2 in different co-solute formulations. The effective viscosity η_{eff} was calculated from the diffusion retardation factor following the length-scale dependent viscosity model[8] ($D_0/D_s = \eta_{eff}/\eta_0$) using D_s obtained from fits of the FCS ACFs to the Gaussian distribution model for 3D diffusion. The hard sphere effective viscosity was calculated from D_0/D_s of hard spheres.[9, 10] Measurements were done in triplicate on dry-passivated glass slides at a focal depth of 3 µm.

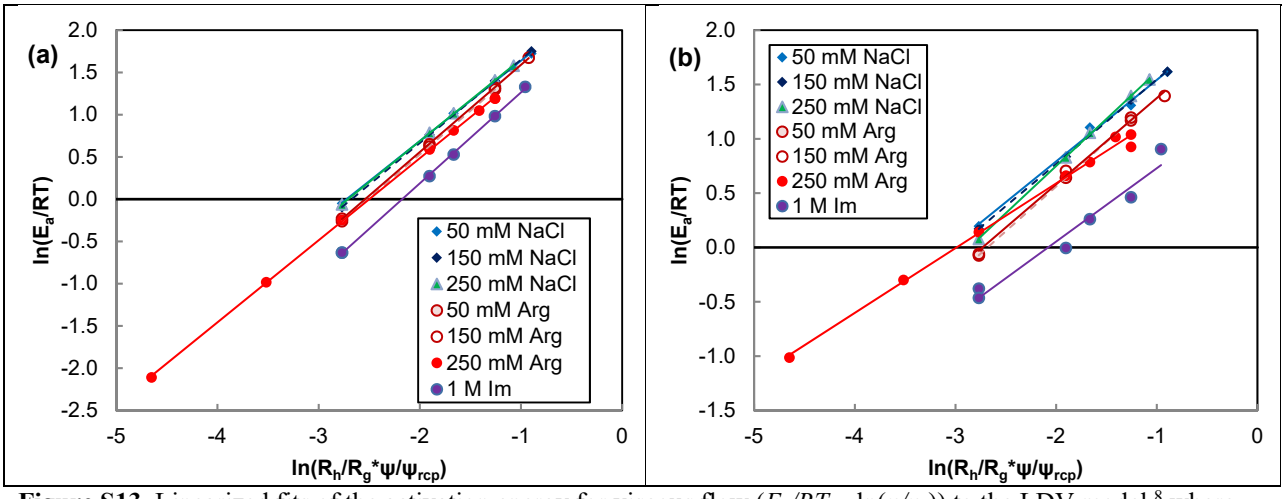

Figure S13. Linearized fits of the activation energy for viscous flow ($E_a/RT = \ln(\eta/\eta_0)$) to the LDV model,[8] where E_a/RT was calculated from the **(a)** macroscopic relative viscosity η_{rel} and **(b)** microscopic relative viscosity ($=D_0/D_s$) for mAb2 in different co-solute formulations. These fits were used to obtain the hydrodynamic parameters a and interaction parameters b reported in Table S4.

Table S4. Fit parameters from the length-scale dependent viscosity model for both the microscopic and macroscopic viscosity for Fig. S13. Given the nearly identical slopes between formulations, average *a* values of 0.80 ± 0.05 and 0.99 ± 0.04 were used for further fits of the microscopic viscosity ($\eta_{eff}/\eta_0 = D_0/D_s$) and macroscopic viscosity, respectively, to the length-scale dependent viscosity model with fixed *a* (Table 3, Fig. S14, Fig. 6). The values of *a* were obtained by averaging over the first 5 rows in the table. Due to the unusual diffusion behavior of 1M Im, as well as the uncertainty and bias in the 250 mM Arg fit caused by the ultralow concentration (10 – 30 mg/mL) data points, these two systems were excluded from the average.

	Fit to microviscosity (D_0/D_s)			**Fit to macroviscosity (η_{rel})**		
Formulation	**a**	**b**	**R^2 of fit**	**a**	**b**	**R^2 of fit**
50 mM NaCl	0.750	9.89	0.995	0.950	13.30	1.000
150 mM NaCl	0.777	10.21	1.000	0.986	13.99	1.000
250 mM NaCl	0.869	12.02	1.000	0.969	13.81	1.000
50 mM Arg.HCl	0.822	9.06	1.000	1.031	13.36	1.000
150 mM Arg.HCl	0.794	8.76	0.996	1.032	13.76	1.000
250 mM Arg.HCl	0.596	5.94	0.995	0.971	11.31	1.000
1 M Imid(HCl)	0.657	4.07	0.960	1.076	10.37	1.000

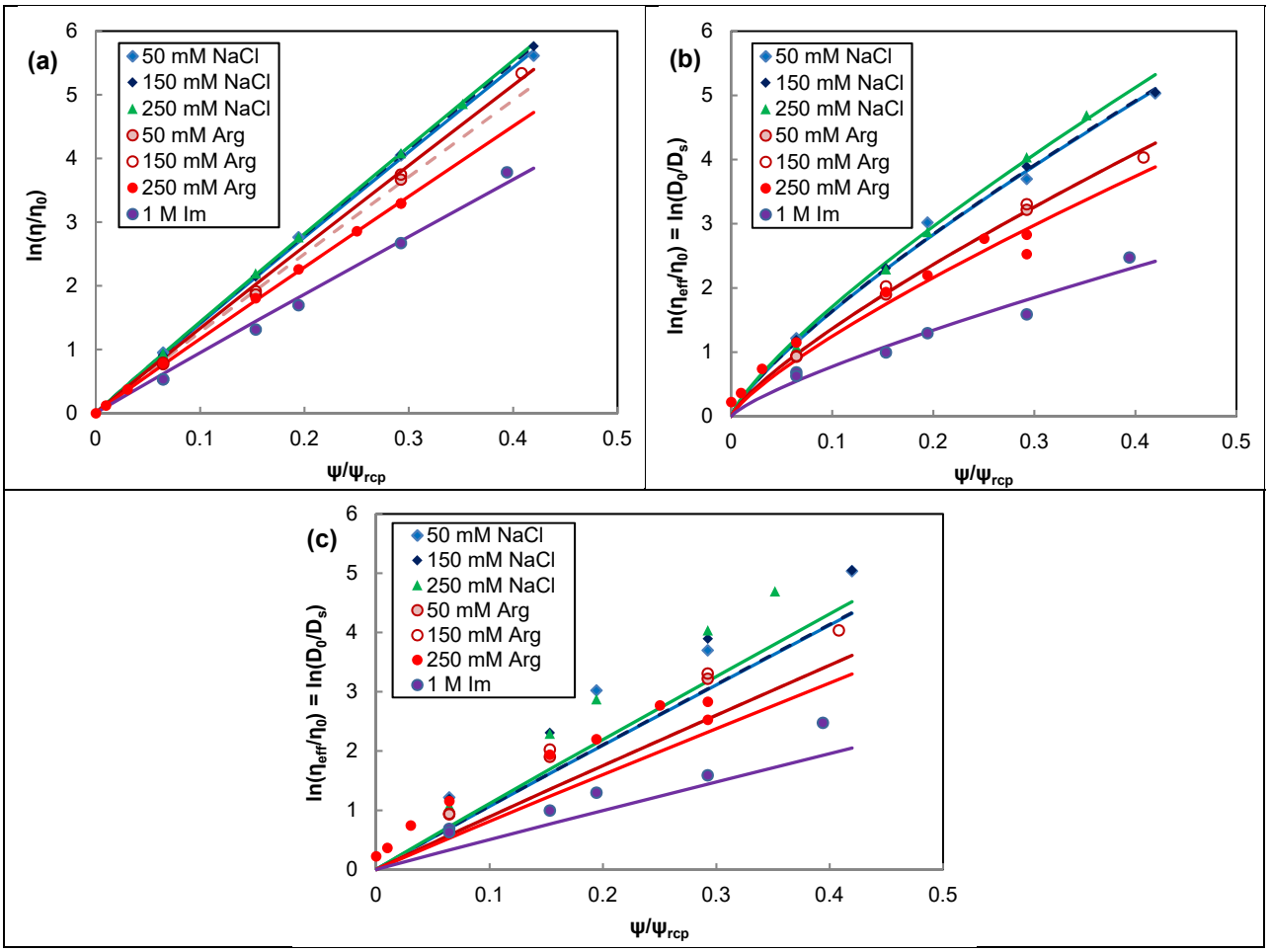

Figure S14. (a) Macroscopic relative viscosity and **(b)** micro (effective) relative viscosity and diffusion retardation as a function of the scaled concentration ψ/ψ_{rcp} for mAb2 in different co-solute formulations. The solid lines are fits of D_0/D_s to the length-scale dependent viscosity model with a fixed a of 0.99 and 0.80 for **(a)** and **(b)** respectively (Table S4) and formulation-dependent fitted values of b (Table 3). **(c)** Poor agreement between the experimental data and the best-fit of the microviscosity (D_0/D_s) to the LDV model using the average a fit from the macroscopic viscosity.

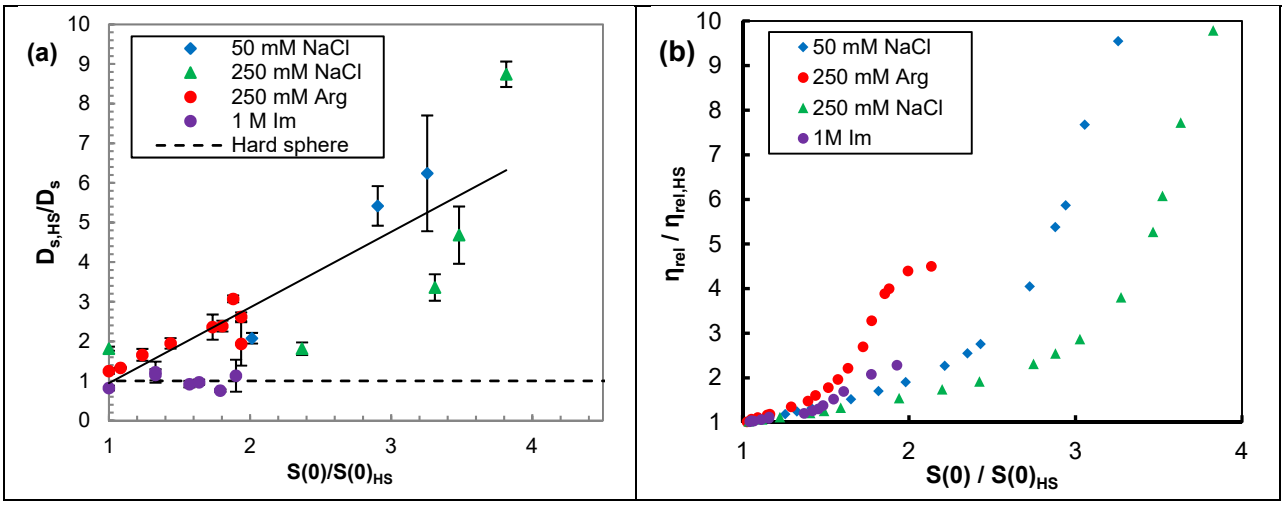

Figure S15. (a) Correlation between the mAb2 hard-sphere normalized self-diffusion $D_{s,HS}/D_s$ and the normalized structure factor $S(0)/S(0)_{HS}$ measured by SLS[11] across multiple co-solute formulations and mAb concentrations from 60 – 200 mg/mL. The 1M Im data was excluded from the linear fit due to the ultrahigh ionic strength and resulting diffusion behavior. **(b)** Relation between mAb2's solution relative viscosity η_{rel} and structure factor $S(0)$, both normalized by the hard sphere (HS) values evaluated at the same concentration (volume fraction) as the mAb solution, as a function of the co-solute formulation.

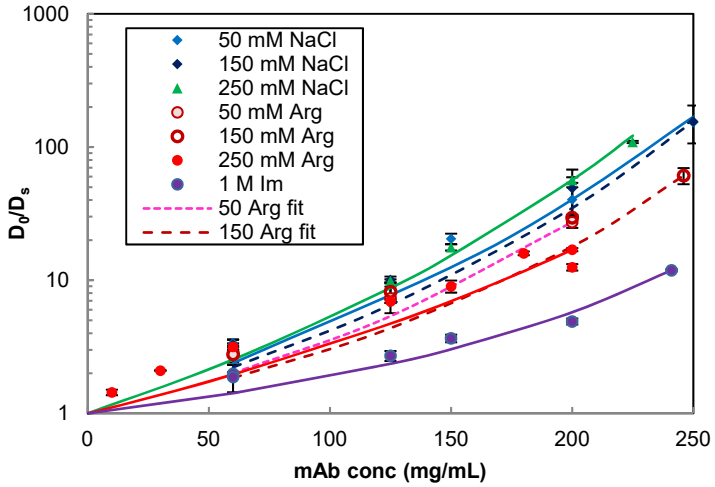

Figure S16. Self-diffusion retardation (microviscosity) of mAb2 as a function of mAb concentration and co-solute (discrete dots) fit to the microviscosity model (Eqn. 16a). The experimental data are shown as discrete points, while the model fits are shown as solid/dashed lines. The fit parameters are reported in Table S5.

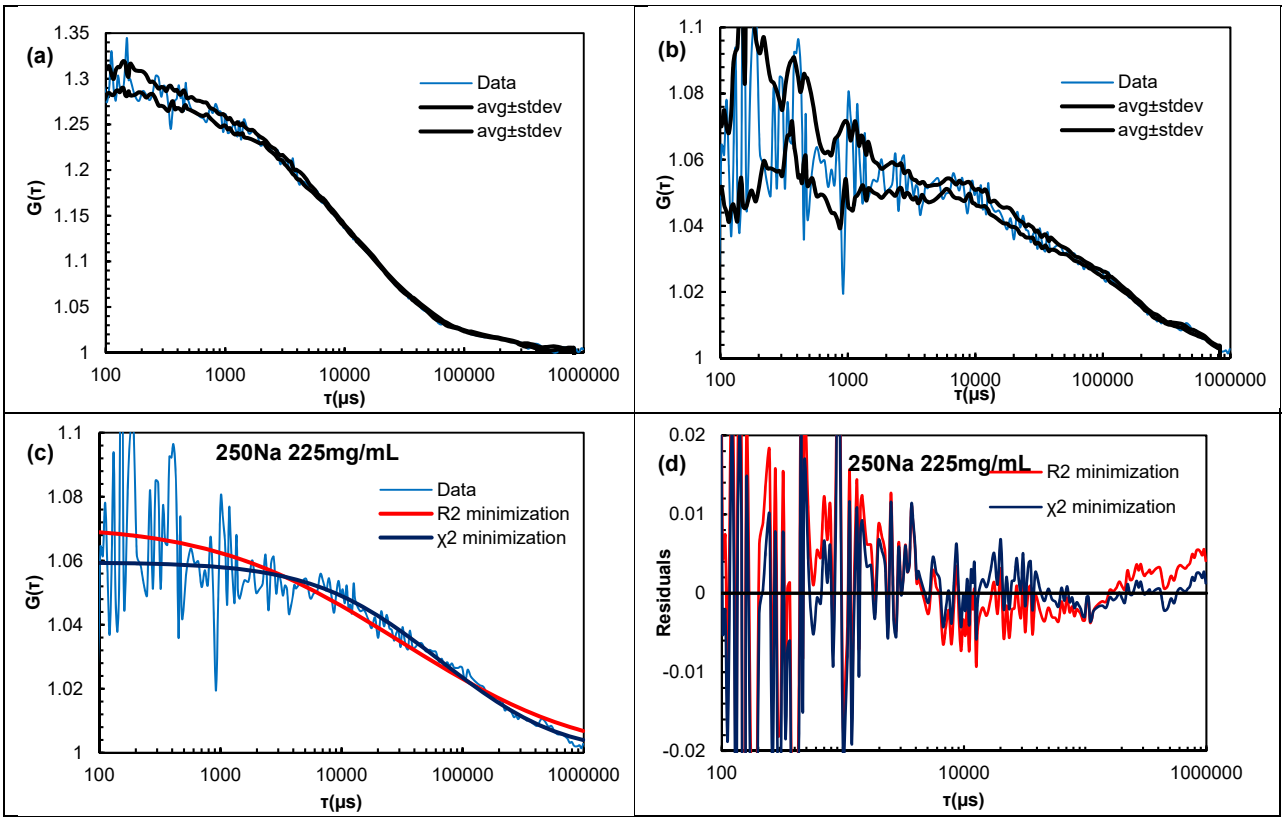

Figure S17. Un-normalized ACFs of mAb2 in 250 mM NaCl at **(a)** 150 mg/mL and **(b)** 225 mg/mL. The bold black lines correspond to the calculated standard deviation in $G(\tau_i)$, which closely approximate the noise in the ACF, and which were used to calculate χ^2. **(c)** Improved fit to the 225 mg/mL ACF and **(d)** reduced residuals at long τ by minimizing χ^2 (reduced weight for noisy data points) instead of R^2.

1. W. T. Snead, C. C. Hayden, A. K. Gadok, C. Zhao, E. M. Lafer, P. Rangamani and J. C. Stachowiak, *Proc. Natl. Acad. Sci. U. S. A.*, 2017, **114**, E3258.
2. J. R. Houser, D. J. Busch, D. R. Bell, B. Li, P. Ren and J. C. Stachowiak, *Soft Matter*, 2016, **12**, 2127-2134.
3. S. D. Chandradoss, A. C. Haagsma, Y. K. Lee, J.-H. Hwang, J.-M. Nam and C. Joo, *Journal of Visualized Experiments : JoVE*, 2014, DOI: 10.3791/50549, 50549.
4. W. Kern, *Journal of The Electrochemical Society*, 1990, **137**, 1887-1892.
5. Z. Yang, J. A. Galloway and H. Yu, *Langmuir*, 1999, **15**, 8405-8411.
6. N. Pal, S. D. Verma, M. K. Singh and S. Sen, *Analytical Chemistry*, 2011, **83**, 7736-7744.
7. H. Yajima, H. Yamamoto, M. Nagaoka, K. Nakazato, T. Ishii and N. Niimura, *Biochim. Biophys. Acta, Gen. Subj.*, 1998, **1381**, 68-76.
8. T. Kalwarczyk, K. Sozanski, S. Jakiela, A. Wisniewska, E. Kalwarczyk, K. Kryszczuk, S. Hou and R. Holyst, *Nanoscale*, 2014, **6**, 10340-10346.
9. M. Roos, M. Ott, M. Hofmann, S. Link, E. Rössler, J. Balbach, A. Krushelnitsky and K. Saalwächter, *Journal of the American Chemical Society*, 2016, **138**, 10365-10372.
10. A. van Blaaderen, J. Peetermans, G. Maret and J. K. G. Dhont, *The Journal of Chemical Physics*, 1992, **96**, 4591-4603.

11. J. J. Hung, B. J. Dear, C. A. Karouta, P. D. Godfrin, J. A. Bollinger, M. P. Nieto, L. R. Wilks, T. Y. Shay, K. Ramachandran, A. Sharma, T. M. Truskett and K. P. Johnston, *J. Phys. Chem. B*, 2019, **123**, 739-755.